Published in final edited form as:
Neuron. 2012 April 12; 74(1): 179–192. doi:10.1016/j.neuron.2012.01.033.

Calcium-Activated Chloride Channels (CaCCs) Regulate Action Potential and Synaptic Response in Hippocampal Neurons

Wendy C. Huang[1,2,4,5], **Shaohua Xiao**[2,5], **Fen Huang**[2], **Brian D. Harfe**[3], **Yuh Nung Jan**[2], and **Lily Yeh Jan**[2,*]

[1]Graduate Program in Neuroscience, University of California, San Francisco, San, Francisco, CA 94158, USA

[2]Departments of Physiology and Biochemistry, Howard Hughes Medical Institute, University of California, San Francisco, San Francisco, CA 94158, USA

[3]Department of Molecular Genetics and Microbiology, The Genetics Institute, University, of Florida, Gainesville, FL 32610, USA

SUMMARY

Central neurons respond to synaptic inputs from other neurons by generating synaptic potentials. Once the summated synaptic potentials reach threshold for action potential firing, the signal propagates leading to transmitter release at the synapse. The calcium influx accompanying such signaling opens calcium-activated ion channels for feedback regulation. Here we report a novel mechanism for modulating hippocampal neuronal signaling that involves calcium-activated chloride channels (CaCCs). We present the first evidence that CaCCs reside in hippocampal neurons and are in close proximity of calcium channels and NMDA receptors to shorten action potential duration, dampen excitatory synaptic potentials, impede temporal summation, and raise the threshold for action potential generation by synaptic potential. Having recently identified TMEM16A and TMEM16B as CaCCs, we further show that TMEM16B but not TMEM16A is important for hippocampal CaCC, laying the groundwork for deciphering the dynamic CaCC modulation of neuronal signaling in neurons important for learning and memory.

INTRODUCTION

Neuronal signaling is subject to feedback regulation by ion channels. A neuron integrates impinging synaptic inputs to generate action potentials for signal transmission to the next neuron; it conveys information by adjusting the action potential number, the “firing frequency,” or timing, the “firing pattern.” As action potential triggers transmitter release from axon terminals, the ensuing transmitter receptor activation leads to synapse responses. Ca^{2+} signals generated during action potential and synaptic potentials activate Ca^{2+}-activated ion channels thereby providing feedback regulation.

Besides voltage-activated Na^+ and K^+ channels that make up the basic machinery for action potential generation (Hodgkin and Huxley, 1952), voltage-gated Ca^{2+} channels open and the

*Correspondence: lily.jan@ucsf.edu.
[4]Present address: Brown University, Providence, RI 02906, USA.
[5]These authors made equal contribution

resultant Ca^{2+} influx activates big-conductance Ca^{2+}-activated K^+ channels (BK) to modulate action potential waveform (Adams et al., 1982; Lancaster and Nicoll, 1987; Storm, 1987a, b), leading to regulation of transmitter release from axon terminals (Hu et al., 2001; Lingle et al., 1996; Petersen and Maruyama, 1984; Raffaelli et al., 2004; Robitaille et al., 1993) and firing patterns in the soma (Madison and Nicoll, 1984; Shao et al., 1999).

As to transmitter activation of glutamatergic α-amino-3-hydroxy-5-methyl-4-isoxazolepropionic acid receptors(AMPA-Rs) and N-methyl D-aspartate receptors (NMDA-Rs), NMDA-Rs mediate Ca^{2+} influx which activates small-conductance Ca^{2+}-activated K^+channels (SK) (Fakler and Adelman, 2008)to influence synaptic plasticity (Lin et al., 2008; Ngo-Anh et al., 2005; Stackman et al., 2002); SK activation during an excitatory postsynaptic potential(EPSP) reduces the synaptic response and the likelihood for long-term potentiation (LTP) (Hammond et al., 2006; Stackman et al., 2002).

Whether and how Ca^{2+}-activated Cl^- channels (CaCCs) might be involved in neuronal signaling is currently unknown. Even the basic question regarding the existence of CaCCs in hippocampal pyramidal neurons has yet to be addressed, notwithstanding earlier studies of CaCCs in anterior pituitary neurons (Korn et al., 1991), amygdala neurons (Sugita et al., 1993) and cingulate cortical neurons (Higashi et al., 1993).

The paucity of information regarding CaCCs in central neurons is partly due to the uncertainty regarding their molecular identity. Now that three independent studies reached the same conclusion that TMEM16A of a family of transmembrane protein with unknown functions encodes a CaCC (Caputo et al., 2008; Schroeder et al., 2008; Yang et al., 2008) – a conclusion verified by reports that the native CaCC current in several cell types is eliminated in TMEM16A knockout mice (Ousingsawat et al., 2009; Romanenko et al., 2010) and TMEM16A is important for vasoconstriction (Manoury et al., 2010), Ca^{2+}-dependent Cl^- transport across airway epithelia (Rock et al., 2009), rhythmic contraction in gastrointestinal tracts (Huang et al., 2009; Hwang et al., 2009) and fluid excretion in salivary glands (Romanenko et al., 2010). Moreover, TMEM16B also gives rise to CaCC (Pifferi et al., 2009; Schroeder et al., 2008), likely accounting for the CaCC in olfactory sensory neurons (Billig et al., 2011; Stephan et al., 2009) and photoreceptor terminals (Barnes and Hille, 1989; Stohr et al., 2009).

In this study, we show CaCCs are present in hippocampal neurons and serve functions important for neuronal signaling. CaCC activation by Ca^{2+} influx through NMDA receptors reduces the EPSP and the extent of temporal summation. CaCC also elevates the threshold for spike generation by excitatory synaptic potentials so as to further dampen EPSP-spike coupling. Ca^{2+} influx through Ca^{2+} channels that open during an action potential activates CaCC to modulate spike duration in the somatodendritic region. Likely encoded by TMEM16B rather than TMEM16A, CaCCs reside in the vicinity of voltage-gated Ca^{2+} channels to regulate spike duration and in close proximity of NMDA receptors to modulate excitatory synaptic responses; both forms of regulation are eliminated by internal BAPTA but not EGTA.

RESULTS

Activating voltage-gated Ca^{2+} channels by depolarizing hippocampal pyramidal neurons induces a tail current that is carried by Cl^- ions

Activation of voltage-gated Ca^{2+} channels can lead to CaCC activation in smooth muscle and sensory neurons (Frings et al., 2000; Scott et al., 1995). To look for CaCC in hippocampal neurons, we applied a 200 ms depolarization step from −70 mV to 0 mV to activate voltage-gated Ca^{2+} channels. This depolarizing prepulse resulted in Ca^{2+} influx due

to the large inward Ca^{2+} current, and was followed by a tail current (arrow, Figure 1A) that reversed near the equilibrium potential of Cl^- ions (E_{Cl}) (Figure 1A, right), in cultured pyramidal neurons at DIV (days *in vitro*) 14 and also in CA1 pyramidal neurons of acute slices from P14–21 (postnatal day 14–21) mice. Only Ca^{2+} and Cl^- ions are possible charge carriers in these experiments because 1) Na^+ was replaced by NMDG and Na^+ channels were blocked by tetrodotoxin (TTX); and 2) K^+ ions were removed and K^+ channels were blocked with Cs^+ and tetraethylamonium (TEA) in the internal solution and 4-aminopyridine (4AP) in the external solution, which also included the $GABA_A$ receptor antagonist picrotoxin (Figure 1A). So we went on to test whether Ca^{2+} influx through Ca^{2+} channels activates Cl^- channels to generate the tail current.

To verify that Cl^- is the ion carrier for the tail current, we determined its reversal potential in three different internal Cl^- concentrations. The voltage steps following the prepulse depolarization ranged from −100 mV to −25 mV (5 or 10 mV steps). After subtracting the background current elicited without a depolarization prepulse (−70 mV holding potential without 0 mV depolarization prepulse) from the tail current elicited with a depolarization prepulse (to 0 mV), we plotted the average tail current measured at 150–200 ms after the end of the 0 mV prepulse as a function of voltage to determine the reversal potential (Figure 1B). We found that the reversal potential, plotted as a function of $\log_{10} [Cl^-]_{in}$, followed the Nernst equation with a slope of 58 mV (Figure 1C). These results reveal that this tail current is a Cl^- current.

The tail current is activated by Ca^{2+}

To verify that this tail Cl^- current is activated by Ca^{2+}, first we eliminated Ca^{2+} current with 100 μM Cd^{2+} (Figure 2A) and found the tail Cl^- current absent (Figure 2A). By including 10 mM BAPTA in the whole cell patch pipette solution to chelate Ca^{2+}, we found that the tail current was nearly abolished (Figure 2B). Moreover, replacing external Ca^{2+} with Ba^{2+} (Figure 2C) also eliminated the tail current (Figure 2C). These experiments demonstrate that the tail current requires internal Ca^{2+} for activation.

To test whether prepulse depolarization to levels approaching the equilibrium potential of Ca^{2+}(E_{Ca}) results in smaller tail current due to the diminishing driving force for Ca^{2+}, we varied the prepulse from −70 mV (no depolarization) to +100 mV and measured the tail current (Figure 2D). Indeed, whereas Ca^{2+} influx was minimal at prepulse potentials more negative than −30 mV due to insufficient activation of Ca^{2+} channels and consequently there was little tail current, the tail current grew with further depolarization and reached a maximum near 0 mV prepulse, and then diminished as the prepulse depolarization approached E_{Ca} (calculated to be > 100 mV).

We next test whether prolonging the prepulse depolarization to increase the Ca^{2+} influx increases the tail current. While the tail current in response to longer prepulse to 0 mV was larger (Figure 2E, white bars), it remained unchanged for prepulse to +100 mV regardless of the duration (Figure 2E, black bars). These experiments show that the tail current is a Ca^{2+}-activated Cl^- current.

CaCC blockers dose-dependently reduce the tail current and broaden the action potential in hippocampal pyramidal neurons

Next, we tested two classical CaCC blockers, niflumic acid (NFA) and 5-nitro-2-(3-phenylpropylamino) benzoic acid (NPPB). Whereas depolarization from −70 mV to 0 mV resulted in an inward Ca^{2+} current followed by a tail current (tail current measured at −90 mV, E_{Cl}= − 46.8 mV), both CaCC blockers reduced the optail current (Figure 3A) while leaving the peak Ca^{2+} current intact.

As shown in Figure 1D for recording from acute slices at 35°C with 2.5 mM external Ca^{2+}, depolarization to 0 mV for one millisecond induced the CaCC tail current that reversed at E_{Cl}. We therefore tested whether CaCC can modulate spike waveform by injecting a 2 ms pulse of current to depolarize neurons in hippocampal slices at 35°C to barely reach the threshold for spike generation ~90% of the time, and looked for the effect of NFA and NPPB. The resting membrane potential ranged from −65 mV to −70 mV in all our experiments, and we injected a small amount of hyperpolarizing current to bring the membrane potential to −70 mV at the start of the experiment. Indeed, 100 μM NFA caused spike broadening (Figure 3B, top); there was a dose-dependent increase of the spike width (measured at 33% of the spike height); with the maximal spike widening corresponding to an increase by ~65% of the control spike width (Figure 3B, bottom). Similar results were obtained with a second CaCC blocker, NPPB (Figure 3C).

The spike broadening following application of 100 μM NFA was reversible upon washout (Supplemental Figure 2A) (see Supplemental Figure 1 for time course plots of drug effects). When we shifted E_{Cl} from −70 mV to +54 mV by changing internal and external Cl^- concentrations, 100 μM NFA narrowed the spike width instead (Supplemental Figure 2B). Importantly, with 10 mM internal BAPTA to chelate Ca^{2+} and prevent CaCC activation, the spike duration was unaffected by NFA (Supplemental Figure 2C). In these and all following studies, the CaCC blockers had no significant effects on the resting membrane potential or input resistance of hippocampal neurons. These controls verify that the observed NFA effect is specific for CaCC, thereby providing support for our conclusion that CaCC controls action potential repolarization.

TMEM16B is expressed in the hippocampus

To explore the molecular identity of the hippocampal CaCC, we performed RT-PCR and found TMEM16B but not TMEM16A transcript in cultured hippocampal neurons (Figure 4A). *In situ* hybridization further revealed that the TMEM16B mRNA is present in CA1 and CA3 pyramidal neurons, dentate granule cells and hilar interneurons of the hippocampus (Figure 4G). We next asked whether the TMEM16B protein is also expressed in the hippocampus, by raising a rabbit polyclonal antibody against an epitope in a putative extracellular loop of mouse TMEM16B. The antibody readily detected TMEM16B-mCherry (monomer ~132 kDa) expressed in HEK293 cells, but not in control cells co-transfected with enzymatically prepared small interfering RNA (esiRNA) targeting TMEM16B (Supplemental Figure 3B). Using this rabbit anti-TMEM16B antibody to probe for the endogenous TMEM16B, we detected a band migrating at the expected size of TMEM16B (~105 kDa) in cultured mouse hippocampal neurons (Figure 4H). These studies reveal that TMEM16B is expressed in the hippocampus.

shRNA knockdown of TMEM16B reduces CaCC and retards action potential repolarization in hippocampal pyramidal neurons

To test for the involvement of TMEM16B in hippocampal CaCC, we cloned two independent small hairpin RNAs (shRNAs) targeting different parts of the TMEM16B mRNA, 16B-shRNAs #2 and #5, as well as a scrambled control shRNA into a lentiviral transfer vector that contains the coding sequence for green fluorescence protein (GFP). These TMEM16B-shRNAs reduced the expression of TMEM16B-mCherry fusion proteins in HEK293 cells (Supplemental Figure 3C) as well as *endogenous* TMEM16B mRNA in cultured hippocampal neurons 10 days after lentivirus infection (Figure 4B). Whereas these infected neurons displayed normal Ca^{2+} current, shRNA #2 or shRNA #5 knockdown of TMEM16B reduced the tail current amplitude by 60 ± 4.5% and 61 ± 5%, respectively, 12 days after infection (Figures 4C and 4D). Significant reduction of the tail current was also observed at 9 and 10 days after infection (Figure 4D). In contrast, comparison of CA1

pyramidal neurons in hippocampal slices from wildtype (n = 7) and TMEM16A KO mice (n = 11) revealed no significant difference in the tail current (109 ± 9% of control with 0 mV prepulse, p = 0.9) (Supplemental Figure 3A), indicating that TMEM16B but not TMEM16A is required for the CaCC in hippocampal pyramidal neurons.

Knockdown of TMEM16B by shRNA #2 or shRNA #5, but not the scrambled control RNA, lengthened the action potential duration by 50 ± 7.6% and 40 ± 5.2% respectively; the action potential broadening was evident starting at 9 days after infection, as well as 10 and 12 days after infection (Figures 4E). We further tested the effect of shRNA knockdown of TMEM16B by performing whole-cell recording of CaCC elicited by raising intracellular Ca^{2+} in the patch pipette solution from 0 to 0.5 μM Ca^{2+}, and found ~80% reduction of CaCC current 10 days after lentivirus infection (Figure 4F). These studies indicate that TMEM16B is important for hippocampal CaCC that regulates the spike waveform.

CaCC shortens action potentials in CA3 pyramidal neurons without affecting transmitter release from their axon terminals

Blocking CaCC caused spike broadening in CA1 and CA3 pyramidal neurons recorded at 35°C (Figures 3B and 5A) and room temperature (Supplemental Figure 4), and the spike broadening persisted in the presence of 100 μM calcium/calmodulin activated kinase II (CaMKII) inhibitor KN62 (Supplemental Figures 4). Whereas 10 mM internal BAPTA prevented CaCC activation following the opening of Ca^{2+} channels (Supplemental Figure 2C and 4A), 100 μM NFA still caused spike broadening when 10 mM EGTA was included in the internal solution (Supplemental Figure 4A), indicating that CaCCs are in close vicinity of voltage-gated Ca^{2+} channels.

We next asked whether CaCC also affects spike duration in the axon terminals. If so, applying CaCC blocker should increase transmitter release from CA3 axon terminals that form synapses with CA1 neurons. First, we performed field recording of the pharmacologically isolated AMPA-fEPSP in the CA1 dendritic field, while stimulating Schaffer collaterals ten times at 10 Hz (Figure 5C). NFA did not alter the AMPA-fEPSPs (106 ± 8.4%, n = 7, p = 0.8). 100 μM NFA also did not alter the pharmacologically isolated NMDA-EPSCs recorded from individual CA1 pyramidal neurons (101 ± 3.1%, n = 5, p = 0.2, Figure 5D) (external Mg^{2+} was removed to facilitate NMDA receptor activation, and 10 mM internal Cl^- was used to minimize the driving force for Cl^- ions when E_{Cl} is −64.4 mV and holding potential is −65 mV). Thus, blocking CaCC alters the action potential waveform in the soma without altering transmitter release, indicating that functional CaCCs reside in somatodendritic regions but not the nerve terminals of CA3 pyramidal neurons.

Ca^{2+} flux through NMDA receptors (NMDA-Rs) activates CaCCs

Next, we asked whether CaCCs are near NMDA-Rs to be activated during synaptic responses. To maximize the chance of detecting CaCC activation during voltage-clamp recording of isolated NMDA-EPSC in the presence of 20 μM CNQX, we replaced external Mg^{2+} with Ca^{2+} and increased the Cl^- driving force by including 130 mM Cl^- in the whole-cell patch pipette solution (E_{Cl} ~ 0 mV) and holding the cell at −65 mV (65 mV driving force), so that CaCC activation would result in Cl^- efflux thus enhancing the NMDA-EPSCs elicited from CA1 pyramidal neurons in acute slices (P14–21) by stimulating Schaffer collaterals every 20 seconds. As shown in Figure 5E, blocking CaCC with NFA reduced the NMDA-EPSC by 28 ± 4.3% (n = 10, p < 0.05), indicating that CaCC is in the vicinity of NMDA-Rs to be activated by the Ca^{2+} influx through NMDA-Rs.

Importantly, when 10 mM of BAPTA was included in the 130 mM Cl^- internal solution, NFA no longer had effect on NMDA-EPSC (100 ± 1.4%, n = 10, p = 0.13, Figure 5F),

providing further evidence that NFA has no presynaptic effect on transmitter release. In contrast, when we included 10 mM EGTA in the patch pipette solution with 130 mM Cl^-, 100 μM NFA still reduced NMDA-EPSC by 32 ± 9% (n = 5, $p < 0.01$, Figure 5G). As summarized in the histogram (Figure 5H), Ca^{2+} influx through NMDA-Rs is capable of activating CaCCs that are in close proximity so that the slower Ca^{2+} chelator EGTA, but not the fast Ca^{2+} chelator BAPTA, allows CaCC activation for feedback modulation of NMDA-EPSCs.

To explore the physiological contribution of CaCCs, first we performed field recording of the pharmacologically isolated NMDA-fEPSP in the CA1 dendritic field in the presence of 2.5 mM Ca^{2+} and 1.3 mM Mg^2. During a 10 Hz stimulation of Schaffer collaterals, the NMDA-fEPSPs gradually increased (Supplemental Figure 5, left). Bath application of NFA enhanced the 3rd, 6th, and 10th (n = 8, 3rd, 138.4 ± 1.5%, $p < 0.01$; 6th, 145 ± 6.6%, $p < 0.01$; 10th, 140 ± 6.4%, $p < 0.01$) but not the 1st NMDA-fEPSP (105 ± 0.5%, n = 8, $p = 0.8$) (Supplemental Figure 5, right), indicating that only when consecutive synaptic responses cause sufficient Ca^{2+} build-up for CaCC activation does NFA exert an effect on the synaptic response.

Next, we recorded the pharmacologically isolated NMDA-EPSPs in CA1 pyramidal neurons while stimulating Schaffer collaterals at 10 Hz, and asked whether CaCC plays a role in NMDA-EPSP spike coupling. In the presence of 10 mM internal Cl^- 100 μM NFA enhanced NMDA-EPSP spike coupling; NMDA-EPSPs summate to spike much later (first spike occurring most frequently at the 10th synaptic response) when CaCC is intact than when CaCC is blocked by 100 μM NFA (first spike occurring most frequently at the 4th or 5th responses) (Supplemental Figure 6A). Thus, when CaCC is blocked by NFA, neurons fire spikes more readily with reduced average latency to first spike and increased average number of spikes per train (Supplemental Figure 6B, n = 10, $p < 0.001$).

The CaCC function depends on the Cl^- concentration gradient because when we elevated the internal Cl^- level to 130 mM ($E_{Cl} \sim 0$ mV), reducing CaCC with 100 μM NFA delayed spike initiation, increased the average latency to first spike and reduced the average number of spikes generated (Supplemental Figures 6C and 6D, n = 10, $p < 0.001$). Thus, whereas CaCC normally acts as an inhibitory brake on NMDA-EPSP to spike coupling, elevating internal Cl^- concentration during neuronal activity or dysfunction could cause CaCC to provide positive feedback and enhance excitation.

CaCC provides a brake to the excitatory synaptic response, temporal summation, and EPSP-spike coupling under physiological conditions at 35°C

To further explore the physiological contribution of CaCCs to synaptic responses, we stimulated Schaffer collaterals at 100–200 microns from the CA1 pyramidal cell body layer every 30 seconds and recorded from CA1 pyramidal neurons at 35°C in physiological solution plus picrotoxin to block $GABA_A$ receptors. Reducing CaCC with 100 μM NFA increased the amplitude of large but not small synaptic potentials (Figure 6A), most likely because the former involved NMDA receptor activation. Indeed, in the presence of 100 μM APV to block NMDA receptors, the EPSP was no longer affected by 100 μM NFA (Figure 5I), regardless the stimulus intensity (Figure 5J).

Under physiological condition with 10 mM $[Cl^-]_{in}$ (Figure 6B, left panel), reducing CaCC with 100 μM NFA amplified EPSPs of large amplitude. In 130 mM $[Cl^-]_{in}$ (Figure 6B, middle panel), however, reducing CaCC with 100 μM NFA dampened EPSPs of large amplitude. NFA had no effect on EPSP amplitude when BAPTA was included with 10 mM $[Cl^-]_{in}$ to chelate Ca^{2+} (Figure 6B, right panel). These controls reinforce the notion that the

NFA block of CaCC affects the large synaptic potentials that involve activation of NMDA-Rs (6 mV EPSP: 147 ± 2.9%, n = 10, $p < 0.05$).

To test whether CaCCs also play a role in EPSP summation to regulate synaptic integration, we delivered 3 nerve stimuli at 40 Hz. Using the ratio of the third EPSP over the first EPSP as a measure of the efficacy of EPSP summation, we observed that reducing CaCC with 100 μM NFA enhanced the summation efficacy by increasing the size of the larger EPSPs (third EPSP) while leaving the first EPSP (EPSPs ≤ 2 mV) unchanged (Figure 6C). While reducing CaCC with 100 μM NFA enhanced EPSP summation under physiological conditions with 10 mM $[Cl^-]_{in}$ (Figure 6D, left panel), 100 μM NFA reduced EPSP summation in 130 mM $[Cl^-]_{in}$ (Figure 6D, middle panel). NFA had no effect on EPSP summation when BAPTA was included with 10 mM $[Cl^-]_{in}$ to chelate Ca^{2+} (Figure 6D, right panel). These controls reinforce the conclusion that CaCC modulates synaptic input integration in hippocampal neurons.

Lastly, to test whether CaCCs contribute to EPSP-spike coupling, we applied five nerve stimuli at 40 Hz. Using nerve stimulation that generated EPSPs too small to reach threshold for spike initiation even with temporal summation in control conditions (Figure 6E, control, black), we found that reducing CaCC activity with 100 μM NFA enhanced EPSP-spike coupling and helped neurons to reach threshold for spike firing (Figure 6E, red). Whereas under physiological conditions with 10 mM $[Cl^-]_{in}$ (Figure 6F, left panel), reducing CaCC with 100 μM NFA enhanced EPSP-spike coupling, in 130 mM $[Cl^-]_{in}$ (Figure 6F, middle panel) 100 μM NFA dampened EPSP-spike coupling. NFA had no effect on EPSP-spike coupling when BAPTA was included with 10 mM $[Cl^-]_{in}$ to chelate Ca^{2+} (Figure 6F, right panel). Thus, CaCC modulates EPSP-spike coupling in a Ca^{2+}-dependent manner (Table 1) by raising the threshold for spike generation by EPSP under physiological conditions, whereas with elevated internal Cl^- CaCC acts to reduce the threshold instead (Table 1).

Taken together, these studies show that CaCC normally acts as an inhibitory brake on action potential duration, EPSP size, EPSP summation as well as EPSP-spike coupling (Table 1). As illustrated in control studies with elevated internal Cl^- (Table 1), raising internal Cl^- concentration during neuronal activity or dysfunction could cause CaCC to provide positive feedback and enhance excitation.

DISCUSSION

This is the first study to document the existence and physiological functions of Ca^{2+}-activated Cl^- channels (CaCCs) in hippocampal pyramidal neurons. In this study, we show that hippocampal pyramidal neurons have functional CaCCs, and their function depends on TMEM16B but not TMEM16A. We have further examined the physiological roles of CaCCs, as summarized below.

The evidence for CaCC in hippocampal pyramidal neurons includes: (1) Activation of voltage-gated Ca^{2+} channels induces a tail current that reverses at E_{Cl} (Figure 1). (2) This Cl^- current is activated by Ca^{2+} and its size varies with the amount of Ca^{2+} influx (Figure 2). (3) The tail current is blocked by two structurally distinct CaCC blockers, NFA and NPPB (Figure 3A). (4) This tail current is greatly reduced by shRNA knockdown of TMEM16B, which encodes a CaCC (Figure 4C and 4D). (5) shRNA knockdown of TMEM16B also eliminates the bulk of the outwardly rectifying, NFA-sensitive, Ca^{2+}-activated Cl^- current of hippocampal neurons (Figure 4F). Notwithstanding the presence of CLC-3 voltage-gated Cl^- channels that require CaMKII for activation in immature hippocampal neurons (Wang et al., 2006), we found spike broadening by CaCC blockers with or without the CaMKII inhibitor KN62, suggesting that the CaCC control of hippocampal neuronal spike waveform is attributable to TMEM16B, but not CLC-3. Given

that shRNA knockdown led to partial removal of TMEM16B, the tail current, and CaCC (Figure 4C–F), it remains possible that CaCC channel proteins other than TMEM16B also contribute to hippocampal CaCC.

Our finding of action potential broadening in hippocampal pyramidal neurons treated with the CaCC blocker NFA or NPPB, or shRNA to knock down TMEM16B, suggests that CaCC shortens spike duration, similar to BK channels (Adams et al., 1982; Lancaster and Nicoll, 1987; Storm, 1987a, b). Interestingly, whereas BK channels regulate transmitter release most likely due to their control of spike waveform in the nerve terminal, blocking CaCCs does not affect transmitter release, indicating a paucity of active CaCCs in the axon terminals. Importantly, Ca^{2+} influx through NMDA-Rs also activates CaCCs, which provide a brake to excitatory synaptic responses, analogous to the actions of the SK type of Ca^{2+}-activated K^+ channels. These findings suggest that CaCCs in somatodendritic regions of hippocampal pyramidal neurons are involved in adjusting the extent of synaptic excitation and controlling the waveform of the action potential.

How could CaCC in hippocampal neurons have escaped notice for so long? Cation channels are the focus of extensive analyses of action potentials in hippocampal neurons, from *in vivo* recordings half a century ago (Kandel and Spencer, 1961) to recent studies (Bean, 2007). Involvement of Cl^- channels was deemed unlikely early on because impaling neurons with KCl-filled electrodes leads to a reversal of inhibitory synaptic potentials without any obvious alteration of the action potential when compared to action potentials recorded with sharp electrodes containing potassium acetate (Storm, 1987a). However, this differential sensitivity may have arisen from a difference in the acetate permeability of different Cl^- channels (Bormann et al., 1987; Hartzell et al., 2005).

CaCC modulates action potential waveform, the size and integration of excitatory synaptic potentials, and EPSP-spike coupling under physiological conditions

Under physiological conditions CaCCs contribute to the modulation of action potential duration, excitatory synaptic response, EPSP summation and EPSP-spike coupling in hippocampal neurons (Table 1). Importantly, in 130 mM $[Cl^-]_{in}$ – with Cl^- current excitatory rather than inhibitory – the CaCC blocker has opposite effects on the action potential and synaptic potentials. Furthermore, inclusion of 10 mM BAPTA to chelate internal Ca^{2+} and prevent CaCC contribution abolished the effect of the CaCC blocker. These control experiments confirm that the observed effects of the CaCC blocker are indeed dependent on both Ca^{2+} and Cl^-. Taken together with the fact that the CaCC blocker had no effect on the resting potential and input resistance of hippocampal neurons, these pharmacological studies provide evidence for CaCC modulation of several physiological functions in hippocampal neurons discussed below.

Action potentials induced by 2 ms current injection under physiological conditions were broadened by blocking CaCC with 100 μM NFA while the voltage threshold remained unchanged (Table 1) – as expected since the brief current injection would not have caused sufficient activation of Ca^{2+} channels and CaCC to alter the threshold, whereas elevating internal Cl^- caused the CaCC blocker NFA to narrow the action potential instead of widening it, also without altering the threshold (Table 1). These experiments further illustrate the flexibility of CaCC modulation as the internal Cl^- level changes with neuronal activity.

Blocking CaCC enhanced the large but not small EPSPs under physiological conditions (Table 1) – because NMDA receptor activation requires sufficient depolarization. Moreover, CaCC activity reduced EPSP summation and raised the threshold of action potentials elicited by stimulating presynaptic axons (Table 1). In contrast to brief depolarization via

current injection, EPSPs of sufficient size to approach threshold would have activated NMDA receptors to open CaCC channels that in turn would influence the spike threshold. Whereas under physiological conditions CaCC acts as a brake to reduce excitatory potential and raise the threshold for synaptic potentials to trigger spike generation, CaCC modulation could change qualitatively – to exaggerate the impact of excitatory synaptic inputs – if the Cl^- driving force is altered by neuronal activity.

Possible physiological implications of CaCC modulation of action potential duration

Controlling action potential duration in different locations of a neuron has different physiological consequences. At the axon terminal, the spike duration dictates the amount of Ca^{2+} influx and the resultant transmitter release (Hu et al., 2001; Lingle et al., 1996; Petersen and Maruyama, 1984; Raffaelli et al., 2004; Robitaille et al., 1993). In the somatodendritic region, the spike waveform determines the firing pattern. We found that CaCCs control the duration of action potentials in the somatodendritic region but not the axon terminals of CA3 pyramidal neurons. Thus, unlike BK, CaCC modulates neuronal signaling by controlling the number of action potentials that can be generated by a burst of synaptic inputs without influencing the signaling strength of each action potential, namely its ability to trigger transmitter release. This finding also indicates that the spike waveform is likely not uniform throughout the neuron, as shown in previous studies (Geiger and Jonas, 2000).

What might be the physiological impact of CaCC modulation of action potential in the somatodendritic region? Given that the CaCCs are activated by Ca^{2+} influx through NMDA receptors, CaCC likely exerts its influence over excitability in the somatodendritic region where an altered spike waveform impacts neuronal signaling in at least two possible ways: firing pattern and coincidence detection.

Changing spike duration can alter the firing pattern, as in the case of BK channels (Madison and Nicoll, 1984; Shao et al., 1999). Not only does the number of action potentials generated during a barrage of synaptic activities dictate the strength of the signal, the message conveyed also depends critically on the temporal pattern of spike firing. We have found that reducing CaCC activity could facilitate the EPSP-spike coupling, causing a short train of synaptic activities to transition from a single spike or no spike at all to a burst of action potentials, indicating that CaCC modulation could adjust neuronal signaling both quantitatively and qualitatively.

Action potentials can back-propagate into the dendrite of hippocampal pyramidal neurons(Hoffman et al., 1997; Migliore et al., 1999). Modulation of the duration of back-propagating action potential invading the dendritic tree is likely to have a strong impact not only on dendritic excitability, but also on coincidence detection of synaptic inputs – the basis of synaptic plasticity. The relative timing between an incoming synaptic potential and a back-propagating spike can determine whether the synapse giving rise to the synaptic potential is potentiated or depressed (Caporale and Dan, 2008; Dan and Poo, 2004). A broader spike could conceivably widen the time window during which a synaptic signal can be potentiated.

Implications of CaCC modulation of EPSP amplitude, EPSP summation, and EPSP-spike coupling

This study provides the first evidence for the involvement of Ca^{2+}-activated Cl^- channels in the negative feedback to rein in the excitatory synaptic responses. Remarkably, NFA block of CaCC increased synaptic potentials in a way similar to the apamin block of SK channels (Ngo-Anh et al., 2005).

Reducing CaCC activity facilitates EPSP summation by leaving the earlier, smaller EPSP intact and amplifying the later, larger EPSPs (Figure 6A, Table 1). This activity-dependent modulation is more nuanced than simple EPSP modulation and has two important implications. 1) CaCC only reins in large EPSPs that have the potential of bringing the neuron to firing an action potential; CaCC acts as a brake, but not on all EPSPs. 2) Once CaCC is activated by Ca^{2+} influx through NMDA-Rs during a barrage of synaptic responses or Ca^{2+} from other cellular processes, the neuronal signaling outcome will be influenced by CaCC modulation of EPSP summation and the threshold for spike generation by EPSP. CaCC thus dynamically gates the information flow between neurons, and it only does so when there are sufficient neuronal activities to raise internal calcium level. In other words, the signaling power of a single EPSP depends on the level of CaCC activation; the extent of CaCC activation by neuronal activities dictates how much a synaptic input actually counts in terms of its ability to generate action potential in one neuron to signal other neurons.

CaCC modulation is qualitatively different when Cl^- gradient is altered

In contrast to physiological conditions with 10 mM $[Cl^-]_{in}$(E_{Cl} near the resting potential), whole cell recording with 130 mM $[Cl^-]_{in}$ revealed that, while the membrane voltage and input resistance remained unchanged, the spike duration is longer and the threshold for spike generation is lowered (Table 1, Supplemental Figure 2). While the former effect is attributable to CaCC, the latter may also involve Cl^- channels that are constitutively active in a resting neuron. Whereas under physiological conditions both K^+ efflux through K^+ channels and Cl^- influx through Cl^- channels that are constitutively active counter sodium channel activation during depolarization in setting the threshold for spike generation, elevating internal Cl^- leads to Cl^- efflux through these Cl^- channels thereby enhancing rather than dampening the excitability.

CaCC modulation may be modified by changes in the Cl^- gradient during physiological and pathological conditions

During normal development, a neuron switches from higher internal Cl^- to lower internal Cl^-, shifting E_{Cl} and converting Cl^- channel activity from excitatory to inhibitory (Ben-Ari, 2002). Whereas most mature neurons normally have low internal Cl^-(5 –10 mM) to allow Cl^- channels to provide inhibition, extended periods of high neuronal activity or pathological conditions such as seizures and brain traumas can lead to accumulation of internal Cl^- and revert Cl^- channel activity back to an excitatory conductance as that during development (Blaesse et al., 2009; De Koninck, 2007; Payne et al., 2003).

The susceptibility of cation-chloride co-transporters to modulation renders the Cl^- gradient a dynamic readout of neuronal activity. For example, in mature hippocampal neurons, spike firing can alter the Cl^- gradient via activity-dependent phosphorylation of KCC2, a K^+-Cl^- co -transporter that normally extrudes Cl^-, resulting in Cl^- accumulation and a positive shift in E_{Cl} (Fiumelli et al., 2005; Woodin et al., 2003). This activity-dependent shift in the Cl^- gradient will cause CaCCs to progressively lose their grip over the action potential duration and threshold for spike initiation by synaptic potentials, as well as EPSP amplitude and summation.

Epilepsy patients exhibit up-regulation of NKCC1 (Cl^- accumulator) and down-regulation of KCC2 (Cl^- extruder) in the temporal lobe, resulting in a positive shift in E_{Cl} (Palma et al., 2006). In hippocampal slices, KCC2 undergoes down-regulation after sustained interictal-like activity in zero-Mg^{2+} conditions (Rivera et al., 2004). Similar positive shift in E_{Cl} due to altered Cl^- gradient also takes place with brain trauma (Bonislawski et al., 2007) and axonal injury (Nabekura et al., 2002). Thus, impairments of Cl^- homeostasis would turn CaCC modulation into positive feedback to further exacerbate the excitotoxicity.

In addition to modulation of the cation-chloride co-transporters, neuronal activities causing extracellular K^+ accumulatioin will result in accumulation of internal Cl^-: High neuronal activity – be it physiological during heightened neuronal activity or pathological during epilepsy or head trauma – depolarizes the cell membrane and activates voltage-gated K^+ channels, leading to K^+ efflux and accumulation of K^+ in the extracellular space (Blaesse et al., 2009). This external K^+ accumulation reduces the driving force for K^+-Cl^- co - transporters, which rely on the K^+ concentration gradient to extrude Cl^-. The resultant Cl^- accumulation inside the cell then shifts E_{Cl} to a more positive voltage, making Cl^- conductance more excitatory.

The fact that CaCC is modulated not only by changing Ca^{2+} levels but also by adjustment of the Cl^- gradient raises intriguing questions as to how CaCC contributes to neuronal signaling under the very relevant physiological and pathological conditions that will lead to dynamic changes of Ca^{2+} and Cl^- levels in hippocampal pyramidal neurons.

EXPERIMENTAL PROCEDURES

Animal Care and Use

The care and use of animals follow the guidelines of the UCSF Institutional Animal Care and Use Committee. C57BL/6 mice were from Charles River Laboratories. TMEM16A knockout mice were provided by Drs. Jason R. Rock and Brian D. Harfe.

Primary Hippocampal Neuron Culture

Hippocampal neurons were isolated from embryonic day 17 C57BL/6 mouse brains, and plated at 2.5–3 × 10^4 cells per cm^2 on poly-L-lysine treated coverslips or culture dishes as described (Fu et al., 2007).

in situ Hybridization

C57BL/6 mice (2–3 months old) were deeply anesthetized and then perfused with 4% paraformaldehyde in 0.1 M phosphate-buffered saline (PBS), pH 7.4, before removing the brain for further fixation in 4% paraformaldehyde/PBS overnight. *in situ* hybridization was performed using a digoxigenin-labeled RNA probe complementary to the mouse *TMEM16B* mRNA, on 20 μm cryostat sections. See Supplemental Experimental Procedures for more details.

RT-PCR and Quantitative RT-PCR

For RT-PCR, total RNA from cultured hippocampal neurons was extracted with Trizol® (Invitrogen). 1–2 μg total RNA was used for cDNA synthesis with SuperScript III First-Strand Synthesis System for RT-PCR (Invitrogen). See Supplemental Experimental Procedures for primers used in PCR amplification.

For quantitative RT-PCR, total RNA was extracted from hippocampal cultures (10^5 cells) with Trizol® LS reagent (Invitrogen) and purified with RNeasy MinElute Kit (Qiagen) following the manufacturers' instructions. All the isolated RNA was used in a reverse transcription reaction to synthesize cDNA using the High Capacity RNA to cDNA Master Mix (Applied Biosystems). Quantitative PCR was performed with Power SYBR Green PCR Master Mix (Applied Biosystems) in the ABI 7900TH Sequence Detection PCR System (Applied Biosystems). Four μL and 0.4 μL of cDNA were used to amplified *TMEM16B* and an internal control *GAPDH*, respectively. Significance of the results was determined using Student's t-test. See Supplemental Experimental Procedures for more details.

TMEM16B Antibody Generation

A rabbit polyclonal antibody was generated against an epitope of mouse TMEM16B protein (QLKEGTQPENSQFDQE) and affinity-purified with the immunizing peptide (Yenzym, South San Francisco, CA).

Protein Extraction and Western Blotting

Hippocampal cultures were lysed for 30 min in a lysis buffer (2% sodium dodecyl sulfate [SDS], 100 mM dithiothreitol, Complete® Proteinase Inhibitor [EDTA-free, Roche Applied Science], and PBS [pH 7.5]). Lysates were centrifuged at 16,000 × g for 10 min. The supernatants were retained for SDS-polyacrylamide gel electrophoresis. Protein samples were resolved with 4–12% polyacrylamide gels, and subsequently electroblotted to polyvinylidene fluoride (PVDF) membranes. Blots were incubated with primary antibodies overnight at 4°C, followed by incubation with HRP-linked secondary antibodies. Signals were visualized using ECL Plus reagent (GE Healthcare) and CL-XPosure Film (Thermo Scientific). The following primary antibodies were used: purified polyclonal rabbit anti-TMEM16B (1:500); mouse anti-α-tubulin (1:1,000, Sigma-Aldrich); mouse anti-β-tubulin (1:1,000, Covance); rabbit anti-DsRed (1:1,000, Clontech).

shRNA and Lentivirus Infection

The target sequences of TMEM16B-shRNA #2, 16B-shRNA #5 and scramble shRNA are 5′-GCCTCCATCTTGTTTATGATT -3′ (clone TRCN0000127010, Open Biosystems), 5′-GCCAGTCATCTGTTTGACAAT -3′ (clone TRCN0000127013, Open Biosystems), and 5′-CCTAAGGTTAAGTCGCCCTCG -3′ (Addgene plasmid 1864) (Sarbassov et al., 2005), respectively. The shRNAs were cloned into pSicoR-GFP lentiviral transfer vector as described by Dr. Tyler Jacks laboratory (http://web.mit.edu/jacks-lab/protocols/pSico.html). Lentiviruses carrying the shRNAs were packaged and concentrated at the UCSF Sandler Center Lentiviral RNAi Core.

Hippocampal cultures (10^5 cells at 4 DIV) were infected with lentiviruses expressing a scrambled shRNA, TMEM16B-shRNA #2 or #5. Tail current and action potential recordings were performed and compared between GFP-expressing neurons 8–12 days after infection. Total RNA was extracted 10 days after infection for quantitative RT-PCR analysis.

Electrophysiology

Hippocampal Culture Recording—Whole-cell recordings were performed on individual cultured pyramidal neurons at 14–21 days *in vitro*. Pyramidal neurons were distinguishable by their relatively large size, lower input resistance (100–200 MΩ), and prominent apical dendrite. The recording pipettes were made from borosilicate glass capillaries (P-97 Sutter Instrument, 1.5 mm/0.86 mm) and pulled on the day of use (3–4 MΩ). All internal solutions have pH 7.2–7.4 and ~300 mosm. All external solutions were made fresh the day of use and adjusted to pH 7.2–7.4 and ~ 300 mosm (measured on the day of use). The bath was constantly perfused with fresh external solution at 2 mL/min throughout the recording, and all experiments were performed at room temperature. The neurons were visualized with a CCD camera (Hamamatsu). Recordings were amplified with MultiClamp 700B (Axon Instruments), and data were analyzed and plotted with Clampfit 10 and ORIGIN. See Supplemental Experimental Procedures for more details.

Acute Hippocampal Slice Recording—Postnatal day 14–21 C57BL/6 mice were anesthetized with isoflurane and decapitated. Brains were removed and submerged in ice-cold sucrose cutting solution (mM): 50 NaCl, 2.5 KCl, 7 $MgCl_2 \cdot 6H_2O$, 0.5 $CaCl_2 \cdot 2H_2O$, 1

$NaH_2PO_4 \cdot H_2O$, 25 $NaHCO_3$, 11 glucose, 150 sucrose, pH 7.2–7.4 after equilibrated with CO_2, ~325–340 mosm. Hippocampal slices ~400 microns thick were prepared using Leica VT1000s vibratome and transferred to a holding chamber for a minimum of 1 hour before use. The holding chamber contained oxygenated (95% O_2-5% CO_2) artificial cerebral spinal fluid (ACSF) (mM): 119 NaCl, 2.5 KCl, 1.3 $MgCl_2$, 2.5 $CaCl_2$, 1 NaH_2PO_4, 26.2 $NaHCO_3$, 11 glucose, pH 7.2–7.4 after CO_2 buffering, ~ 300 mosm.

Bipolar stimulating electrode was placed in *stratum radiatum* to stimulate the Schaffer collaterals (axons of CA3 neurons) and whole-cell recordings from the cell bodies of CA1 pyramidal neurons were obtained. The external bath solution was oxygenated with 95% O_2-5%CO_2 and the slices were continually perfused at 2 mL/min in room temperature or 35°C. The neurons were visualized with a CCD camera (Hamamatsu). Recordings were performed with patch clamp amplifiers (MultiClamp 700B, Axon Instruments), and data were analyzed and plotted with Clampfit 10 and ORIGIN. See Supplemental Experimental Procedures for more details.

Supplementary Material

Refer to Web version on PubMed Central for supplementary material.

Acknowledgments

We thank Roger Nicoll, Yuriy Kirichok, Michael Stryker, Woo-Ping Ge, Jim Berg, Shi-Bing Yang, Huanghe Yang and Ye He for helpful discussions throughout this work. We thank the UCSF Sandler Center Lentiviral RNAi Core for the assistance with the shRNA experiments. This work was supported by grants MH065334 and NS069229 from National Institute of Health. Y. N. J. and L. Y. J. are HHMI investigators.

References

Adams PR, Constanti A, Brown DA, Clark RB. Intracellular Ca^{2+} activates a fast voltage-sensitive K^+ current in vertebrate sympathetic neurones. Nature. 1982; 296:746–749. [PubMed: 6280066]

Barnes S, Hille B. Ionic channels of the inner segment of tiger salamander cone photoreceptors. J Gen Physiol. 1989; 94:719–743. [PubMed: 2482325]

Bean BP. The action potential in mammalian central neurons. Nat Rev Neurosci. 2007; 8:451–465. [PubMed: 17514198]

Ben-Ari Y. Excitatory actions of gaba during development: the nature of the nurture. Nat Rev Neurosci. 2002; 3:728–739. [PubMed: 12209121]

Billig GM, Pal B, Fidzinski P, Jentsch TJ. Ca^{2+}-activated Cl^- currents are dispensable for olfaction. Nat Neurosci. 2011

Blaesse P, Airaksinen MS, Rivera C, Kaila K. Cation-chloride cotransporters and neuronal function. Neuron. 2009; 61:820–838. [PubMed: 19323993]

Bonislawski DP, Schwarzbach EP, Cohen AS. Brain injury impairs dentate gyrus inhibitory efficacy. Neurobiol Dis. 2007; 25:163–169. [PubMed: 17045484]

Bormann J, Hamill OP, Sakmann B. Mechanism of anion permeation through channels gated by glycine and gamma-aminobutyric acid in mouse cultured spinal neurones. J Physiol. 1987; 385:243–286. [PubMed: 2443667]

Caporale N, Dan Y. Spike timing-dependent plasticity: a Hebbian learning rule. Annu Rev Neurosci. 2008; 31:25–46. [PubMed: 18275283]

Caputo A, Caci E, Ferrera L, Pedemonte N, Barsanti C, Sondo E, Pfeffer U, Ravazzolo R, Zegarra-Moran O, Galietta LJ. TMEM16A, a membrane protein associated with calcium-dependent chloride channel activity. Science. 2008; 322:590–594. [PubMed: 18772398]

Dan Y, Poo MM. Spike timing-dependent plasticity of neural circuits. Neuron. 2004; 44:23–30. [PubMed: 15450157]

De Koninck Y. Altered chloride homeostasis in neurological disorders: a new target. Curr Opin Pharmacol. 2007; 7:93–99. [PubMed: 17182282]

Fakler B, Adelman JP. Control of K_{Ca} channels by calcium nano/microdomains. Neuron. 2008; 59:873–881. [PubMed: 18817728]

Fiumelli H, Cancedda L, Poo MM. Modulation of GABAergic transmission by activity via postsynaptic Ca^{2+}-dependent regulation of KCC2 function. Neuron. 2005; 48:773–786. [PubMed: 16337915]

Frings S, Reuter D, Kleene SJ. Neuronal Ca^{2+}-activated Cl^{-} channels--homing in on an elusive channel species. Prog Neurobiol. 2000; 60:247–289. [PubMed: 10658643]

Geiger JR, Jonas P. Dynamic control of presynaptic Ca^{2+} inflow by fast-inactivating K^{+} channels in hippocampal mossy fiber boutons. Neuron. 2000; 28:927–939. [PubMed: 11163277]

Hammond RS, Bond CT, Strassmaier T, Ngo-Anh TJ, Adelman JP, Maylie J, Stackman RW. Small-conductance Ca^{2+}-activated K^{+} channel type 2 (SK2) modulates hippocampal learning, memory, and synaptic plasticity. J Neurosci. 2006; 26:1844–1853. [PubMed: 16467533]

Hartzell C, Putzier I, Arreola J. Calcium-activated chloride channels. Annu Rev Physiol. 2005; 67:719–758. [PubMed: 15709976]

Higashi H, Tanaka E, Inokuchi H, Nishi S. Ionic mechanisms underlying the depolarizing and hyperpolarizing afterpotentials of single spike in guinea-pig cingulate cortical neurons. Neuroscience. 1993; 55:129–138. [PubMed: 8350984]

Hodgkin AL, Huxley AF. Propagation of electrical signals along giant nerve fibers. Proc R Soc Lond B Biol Sci. 1952; 140:177–183. [PubMed: 13003922]

Hoffman DA, Magee JC, Colbert CM, Johnston D. K^{+} channel regulation of signal propagation in dendrites of hippocampal pyramidal neurons. Nature. 1997; 387:869–875. [PubMed: 9202119]

Hu H, Shao LR, Chavoshy S, Gu N, Trieb M, Behrens R, Laake P, Pongs O, Knaus HG, Ottersen OP, et al. Presynaptic Ca^{2+}-activated K^{+} channels in glutamatergic hippocampal terminals and their role in spike repolarization and regulation of transmitter release. J Neurosci. 2001; 21:9585–9597. [PubMed: 11739569]

Huang F, Rock JR, Harfe BD, Cheng T, Huang X, Jan YN, Jan LY. Studies on expression and function of the TMEM16A calcium-activated chloride channel. Proc Natl Acad Sci U S A. 2009; 106:21413–21418. [PubMed: 19965375]

Hwang SJ, Blair PJ, Britton FC, O'Driscoll KE, Hennig G, Bayguinov YR, Rock JR, Harfe BD, Sanders KM, Ward SM. Expression of anoctamin 1/TMEM16A by interstitial cells of Cajal is fundamental for slow wave activity in gastrointestinal muscles. J Physiol. 2009; 587:4887–4904. [PubMed: 19687122]

Kandel ER, Spencer WA. Electrophysiology of hippocampal neurons. II. After-potentials and repetitive firing. J Neurophysiol. 1961; 24:243–259. [PubMed: 13751138]

Kimura N, Tamura T, Murakami M. Evaluation of the performance of two carbodiimide-based cyanine dyes for detecting changes in mRNA expression with DNA microarrays. Biotechniques. 2005; 38:797–806. [PubMed: 15945376]

Kittler R, Heninger AK, Franke K, Habermann B, Buchholz F. Production of endoribonuclease-prepared short interfering RNAs for gene silencing in mammalian cells. Nat Methods. 2005; 2:779–784. [PubMed: 16179925]

Korn SJ, Bolden A, Horn R. Control of action potentials and Ca^{2+} influx by the Ca^{2+}-dependent chloride current in mouse pituitary cells. J Physiol. 1991; 439:423–437. [PubMed: 1654415]

Lancaster B, Nicoll RA. Properties of two calcium-activated hyperpolarizations in rat hippocampal neurones. J Physiol. 1987; 389:187–203. [PubMed: 2445972]

Lin MT, Lujan R, Watanabe M, Adelman JP, Maylie J. SK2 channel plasticity contributes to LTP at Schaffer collateral-CA1 synapses. Nat Neurosci. 2008; 11:170–177. [PubMed: 18204442]

Lingle CJ, Solaro CR, Prakriya M, Ding JP. Calcium-activated potassium channels in adrenal chromaffin cells. Ion Channels. 1996; 4:261–301. [PubMed: 8744211]

Madison DV, Nicoll RA. Control of the repetitive discharge of rat CA1 pyramidal neurones in vitro. J Physiol. 1984; 354:319–331. [PubMed: 6434729]

Manoury B, Tamuleviciute A, Tammaro P. TMEM16A/anoctamin 1 protein mediates calcium-activated chloride currents in pulmonary arterial smooth muscle cells. J Physiol. 2010; 588:2305–2314. [PubMed: 20421283]

Migliore M, Hoffman DA, Magee JC, Johnston D. Role of an A-type K^+ conductance in the back-propagation of action potentials in the dendrites of hippocampal pyramidal neurons. J Comput Neurosci. 1999; 7:5–15. [PubMed: 10481998]

Nabekura J, Ueno T, Okabe A, Furuta A, Iwaki T, Shimizu-Okabe C, Fukuda A, Akaike N. Reduction of KCC2 expression and $GABA_A$ receptor-mediated excitation after in vivo axonal injury. J Neurosci. 2002; 22:4412–4417. [PubMed: 12040048]

Ngo-Anh TJ, Bloodgood BL, Lin M, Sabatini BL, Maylie J, Adelman JP. SK channels and NMDA receptors form a Ca^{2+}-mediated feedback loop in dendritic spines. Nat Neurosci. 2005; 8:642–649. [PubMed: 15852011]

Palma E, Amici M, Sobrero F, Spinelli G, Di Angelantonio S, Ragozzino D, Mascia A, Scoppetta C, Esposito V, Miledi R, et al. Anomalous levels of Cl^- transporters in the hippocampal subiculum from temporal lobe epilepsy patients make GABA excitatory. Proc Natl Acad Sci U S A. 2006; 103:8465–8468. [PubMed: 16709666]

Payne JA, Rivera C, Voipio J, Kaila K. Cation-chloride co-transporters in neuronal communication, development and trauma. Trends Neurosci. 2003; 26:199–206. [PubMed: 12689771]

Petersen OH, Maruyama Y. Calcium-activated potassium channels and their role in secretion. Nature. 1984; 307:693–696. [PubMed: 6321995]

Pifferi S, Dibattista M, Menini A. TMEM16B induces chloride currents activated by calcium in mammalian cells. Pflugers Arch. 2009; 458:1023–1038. [PubMed: 19475416]

Raffaelli G, Saviane C, Mohajerani MH, Pedarzani P, Cherubini E. BK potassium channels control transmitter release at CA3-CA3 synapses in the rat hippocampus. J Physiol. 2004; 557:147–157. [PubMed: 15034127]

Rivera C, Voipio J, Thomas-Crusells J, Li H, Emri Z, Sipila S, Payne JA, Minichiello L, Saarma M, Kaila K. Mechanism of activity-dependent downregulation of the neuron-specific K-Cl cotransporter KCC2. J Neurosci. 2004; 24:4683–4691. [PubMed: 15140939]

Robitaille R, Garcia ML, Kaczorowski GJ, Charlton MP. Functional colocalization of calcium and calcium-gated potassium channels in control of transmitter release. Neuron. 1993; 11:645–655. [PubMed: 7691106]

Rock JR, O'Neal WK, Gabriel SE, Randell SH, Harfe BD, Boucher RC, Grubb BR. Transmembrane protein 16A (TMEM16A) is a Ca^{2+}-regulated Cl^- secretory channel in mouse airways. J Biol Chem. 2009; 284:14875–14880. [PubMed: 19363029]

Romanenko VG, Catalan MA, Brown DA, Putzier I, Hartzell HC, Marmorstein AD, Gonzalez-Begne M, Rock JR, Harfe BD, Melvin JE. Tmem16A encodes the Ca^{2+}-activated Cl^- channel in mouse submandibular salivary gland acinar cells. J Biol Chem. 2010; 285:12990–13001. [PubMed: 20177062]

Sarbassov DD, Guertin DA, Ali SM, Sabatini DM. Phosphorylation and regulation of Akt/PKB by the rictor-mTOR complex. Science. 2005; 307:1098–1101. [PubMed: 15718470]

Schroeder BC, Cheng T, Jan YN, Jan LY. Expression cloning of TMEM16A as a calcium-activated chloride channel subunit. Cell. 2008; 134:1019–1029. [PubMed: 18805094]

Scott RH, Sutton KG, Griffin A, Stapleton SR, Currie KP. Aspects of calcium-activated chloride currents: a neuronal perspective. Pharmacol Ther. 1995; 66:535–565. [PubMed: 7494858]

Shao LR, Halvorsrud R, Borg-Graham L, Storm JF. The role of BK-type Ca^{2+}-dependent K^+ channels in spike broadening during repetitive firing in rat hippocampal pyramidal cells. J Physiol. 1999; 521(Pt 1):135–146. [PubMed: 10562340]

Stackman RW, Hammond RS, Linardatos E, Gerlach A, Maylie J, Adelman JP, Tzounopoulos T. Small conductance Ca^{2+}-activated K^+ channels modulate synaptic plasticity and memory encoding. J Neurosci. 2002; 22:10163–10171. [PubMed: 12451117]

Stephan AB, Shum EY, Hirsh S, Cygnar KD, Reisert J, Zhao H. ANO2 is the cilial calcium-activated chloride channel that may mediate olfactory amplification. Proc Natl Acad Sci U S A. 2009; 106:11776–11781. [PubMed: 19561302]

Stohr H, Heisig JB, Benz PM, Schoberl S, Milenkovic VM, Strauss O, Aartsen WM, Wijnholds J, Weber BH, Schulz HL. TMEM16B, a novel protein with calcium-dependent chloride channel activity, associates with a presynaptic protein complex in photoreceptor terminals. J Neurosci. 2009; 29:6809–6818. [PubMed: 19474308]

Storm JF. Action potential repolarization and a fast after-hyperpolarization in rat hippocampal pyramidal cells. J Physiol. 1987a; 385:733–759. [PubMed: 2443676]

Storm JF. Intracellular injection of a Ca^{2+} chelator inhibits spike repolarization in hippocampal neurons. Brain Res. 1987b; 435:387–392. [PubMed: 3123013]

Sugita S, Tanaka E, North RA. Membrane properties and synaptic potentials of three types of neurone in rat lateral amygdala. J Physiol. 1993; 460:705–718. [PubMed: 8487215]

Wang XQ, Deriy LV, Foss S, Huang P, Lamb FS, Kaetzel MA, Bindokas V, Marks JD, Nelson DJ. CLC-3 channels modulate excitatory synaptic transmission in hippocampal neurons. Neuron. 2006; 52:321–333. [PubMed: 17046694]

Woodin MA, Ganguly K, Poo MM. Coincident pre- and postsynaptic activity modifies GABAergic synapses by postsynaptic changes in Cl- transporter activity. Neuron. 2003; 39:807–820. [PubMed: 12948447]

Yang YD, Cho H, Koo JY, Tak MH, Cho Y, Shim WS, Park SP, Lee J, Lee B, Kim BM, et al. TMEM16A confers receptor-activated calcium-dependent chloride conductance. Nature. 2008; 455:1210–1215. [PubMed: 18724360]

HIGHLIGHTS

- There *are* calcium-activated chloride channels (CaCCs) in hippocampal pyramidal neurons
- CaCCs shorten action potential duration
- CaCCs dampen EPSP synaptic response, impede summation, and raise threshold for EPSP-spike coupling
- TMEM16B, not TMEM16A, is important for CaCC function in hippocampal pyramidal neurons

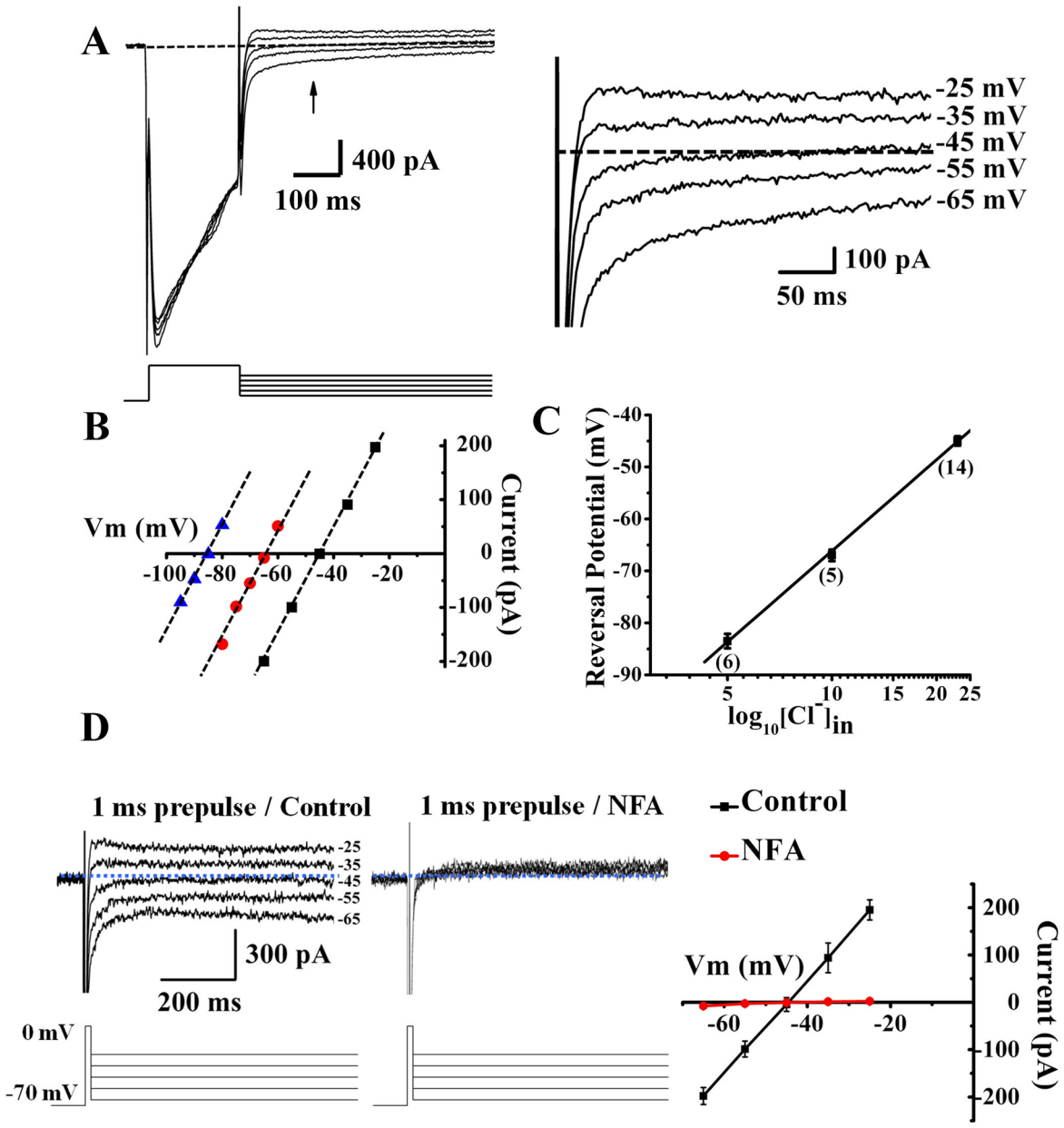

Figure 1.

The tail current induced by Ca^{2+} channel activation in cultured hippocampal pyramidal neurons is a Cl^- current. (A) Depolarization (at room temperature for A-C) to 0 mV for 200 ms results in Ca^{2+} current followed by a tail current that reverses at E_{Cl}. (B) The reversal potential follows E_{Cl}: black, 23 mM $[Cl^-]_{in}$(E_{Cl}= −46.8 mV), red, 10 mM $[Cl^-]_{in}$(E_{Cl}= −67.8 mV), blue, 5 mM $[Cl^-]_{in}$(E_{Cl}= −85.3 mV). (C) The average reversal potential is −45.1 ± 0.9 mV at 23 mM $[Cl^-]_{in}$ (n = 14), −67.2 ± 1.1 mV at 10 mM $[Cl^-]_{in}$ (n = 5), and −83.5 ± 1.4 mV at 5 mM $[Cl^-]_{in}$ (n = 6). (D) Depolarizing neurons (in acute slices at 35°C with 2.5 mM Ca^{2+}) to 0 mV for 1 ms results in Ca^{2+} current followed by a tail current that reverses at E_{Cl} as in the case of cultured neurons: −45 ± 0.5 mV (n = 25 for 10 recordings from cultured neurons and 15 from acute slices) (E_{Cl}= −46.8 mV). The tail (left) is sensitive

to the CaCC blocker NFA (300 μM) (middle). The dashed line in A and D indicates zero current. See Supplemental Figure 1A for time course plot.

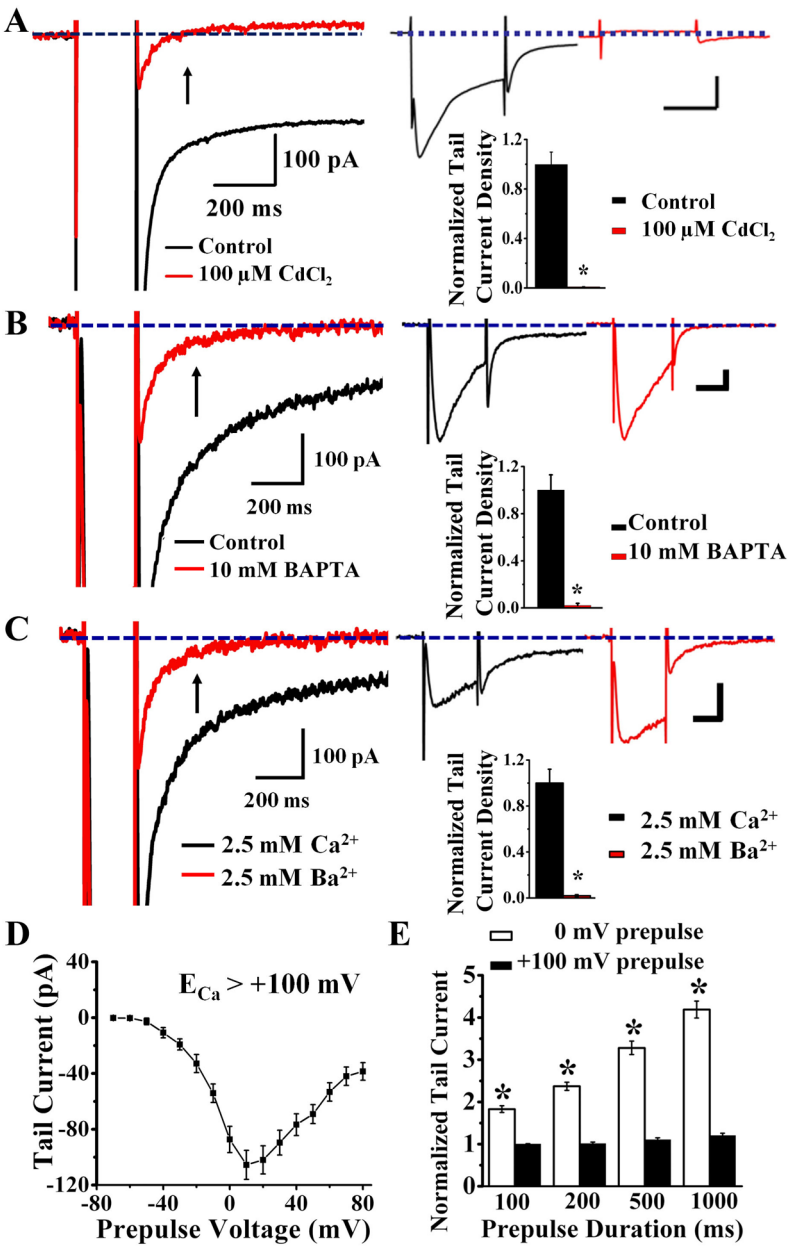

Figure 2.

The tail current recorded at room temperature from cultured hippocampal pyramidal neurons is a Ca^{2+}-activated Cl^- current. (A) 100 μM $CdCl_2$ eliminates tail current (left) by blocking Ca^{2+} current (right top, red). The Cl^- tail current requires Ca^{2+} for activation (black) (right bottom)(n = 10, $p < 0.01$). See Supplemental Figure 1B for time course plot. (B) 10 mM BAPTA in the pipette solution left Ca^{2+} current intact (right top, red) but eliminated tail current (left) (right bottom)(red, n = 12, $p < 0.01$).(C) With external 2.5 mM Ca^{2+} replaced by 2.5 mM Ba^{2+}, Ba^{2+} ions that carry the inward current (right top, red) cannot activate the Cl^- tail current (right bottom)(n = 13, $p < 0.01$). For A–C, scale bar for right top panel is 100 ms, 200 pA, and arrow points to the 150–200 ms time window where the average tail current measurement is taken. See Supplemental Figure 1C for time course plot. (D) Tail current diminishes in amplitude as prepulse voltage approaches E_{Ca} (> + 100 mV) (n = 52).

(E) Tail current increases with increasing duration of prepulse to 0 mV ($n = 22$, $p < 0.01$) but not + 100 mV ($n = 22$, $p = 0.9$).

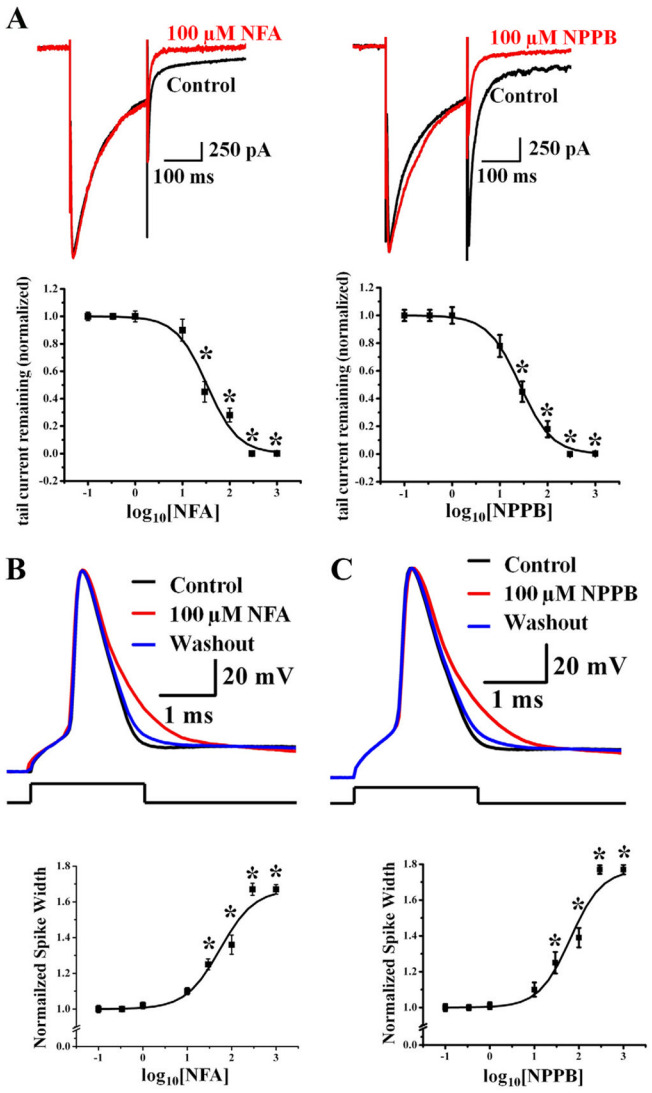

Figure 3.

Ca^{2+}-activated Cl^{-} current in hippocampal pyramidal neurons is sensitive to two different CaCC blockers and is important for controlling action potential duration. (A) CaCC is significantly reduced to 28 ± 5.1% of control by 100 μM NFA (top left, n = 9, $p < 0.001$) and to 18 ± 5.9% of control by 100 μM NPPB (top right, n = 10, $p < 0.001$). IC50 is 33 ± 2.3 μM for NFA (bottom left, n = 5), and 26.2 ± 1.36 μM for NPPB (bottom right, sequentially increasing blocker concentration at room temperature, n = 5). The membrane voltage was held at −70 mV, depolarized to 0 mV to induce Ca^{2+} influx and repolarized back to −90 mV to elicit Ca^{2+}-activated Cl^{-} current. * $p < 0.01$. See Supplemental Figure 1D and 1E for time course plots. (B) Reducing CaCC with 100 μM NFA (red) causes the spike width to increase by ~30% compared to action potentials prior to NFA application (control, black) and after washout of NFA (blue) (top panel). A single action potential is elicited by injecting 2-ms current barely reaching threshold for neurons in acute slices at 35°C in B and C. Bottom panel shows the dose response curve for NFA, which was applied at increasing concentrations sequentially (n = 5). The dose for half maximal spike widening (measured at 1/3 total spike height) is 55.08 ± 5.72 μM NFA; the maximal spike widening corresponds to an increase of the spike width by ~65%. * $p < 0.05$. See Supplemental Figure 1F for time

course plot and experimental details and Supplemental Figure 4 for CaMKII inhibitor control. (C) Apply 100 μM NPPB caused the spike width to increase by ~30% (control, black; NPPB, red; washout, blue) (top panel). Bottom panel shows the dose response curve for NPPB (n = 5). The dose for half maximal spike widening (measured at 1/3 total spike height) is 48.07 ± 10.22 μM; the maximal spike widening corresponds to an increase of the spike width by ~70%. * $p < 0.05$. See Supplemental Figure 1G for time course plot and experimental details.

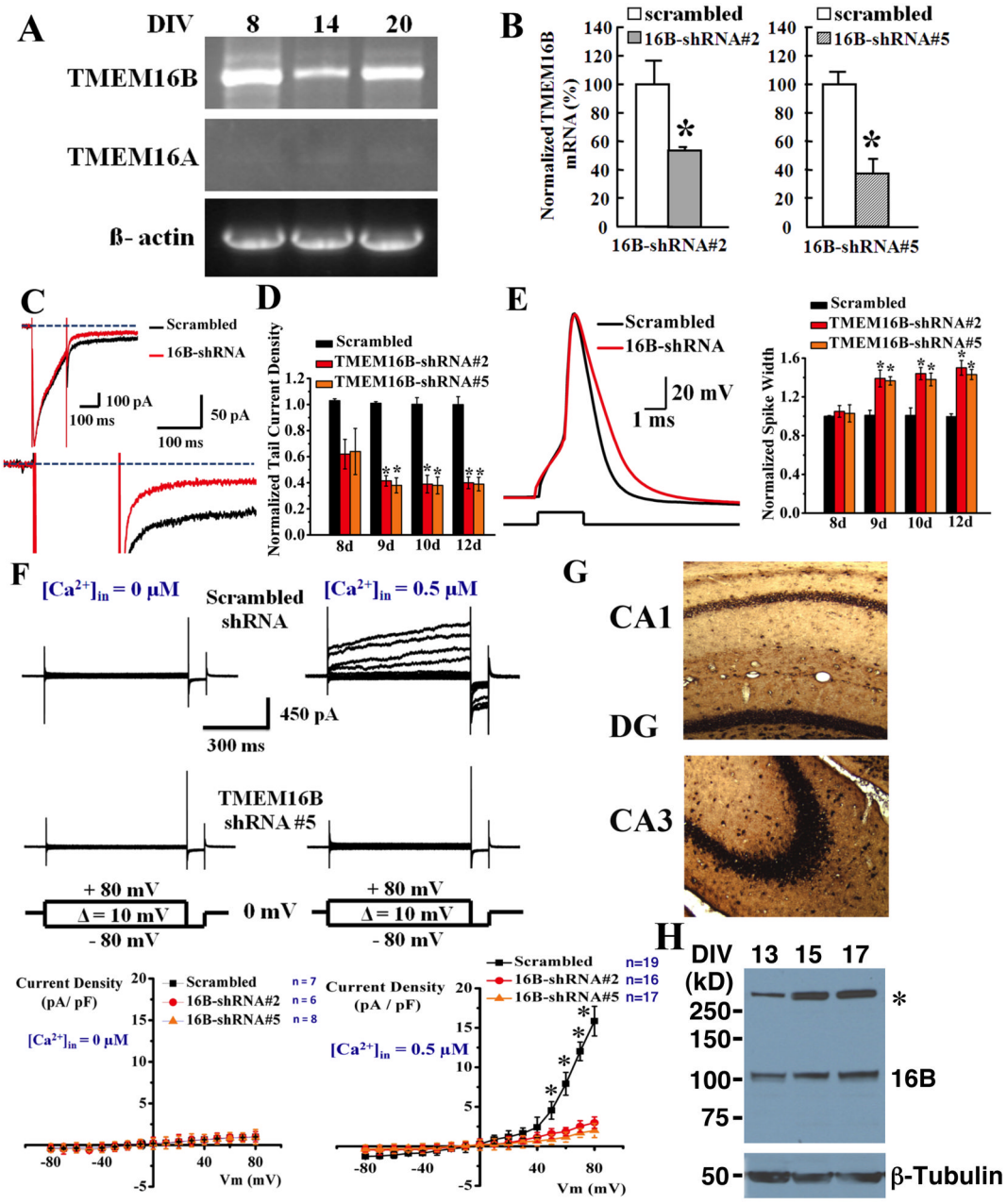

Figure 4.

TMEM16B is expressed in hippocampal pyramidal neurons and is important for the control of action potential duration and the generation of CaCC. (A) RT-PCR reveals TMEM16B (top) but not TMEM16A (middle) expression in neurons 8, 14, and 20 days *in vitro* (DIV). β-actin is included as loading control (bottom). (B) Quantitative RT-PCR revealed that 16B-shRNAs #2 (left) and #5 (right) reduced the expression of TMEM16B mRNA to 54 ± 1.0% (n = 3) and 37 ± 5.5% (n = 3) of scrambled shRNA control respectively. * $p < 0.05$. See Supplemental Figure 3C for additional control for knockdown of TMEM16B expression by 16B-shRNA #2 and #5. (C) CaCC tail current from cultured hippocampal pyramidal neurons at room temperature is significantly reduced (by 67.5%) by TMEM16B shRNA knockdown (red), but not by scrambled RNA control (black). Inset (top left): TMEM16B knockdown does not affect the Ca^{2+} current. (D) Ca^{2+}-activated Cl^{-} current is reduced by 60 ± 4.5% and

61 ± 5% by TMEM16B shRNA #2 and #5, respectively (scrambled, n = 17, shRNA #2, n = 18, $p < 0.01$, shRNA #5, n = 12, $p < 0.01$, 12 days after infection). (E) Left, TMEM16B shRNA #2 knockdown broadens spike waveform (red) as compared to scrambled RNA control (black) (12 days after infection). Right, summary of the effect of TMEM16B-shRNA #2 and #5 on action potential duration (resting potential ~65 mV). (F) In neurons recorded (with ~140 mM Cl^- on both sides) at 35°C 10 days after infection with lentivirus for scrambled shRNA (top panels), raising intracellular Ca^{2+} from 0 (left) to 0.5 μM Ca^{2+}(right) gives rise to CaCC that is blocked by 300 μM NFA. This CaCC current was greatly reduced in neurons infected with shRNA #5 (middle panels). Current-voltage curves (bottom panels) plotted for current recorded by applying voltage steps from −80 to +80 mV (10 mV intervals) from holding potential of 0 mV ($E_{Cl} = 0$) without intracellular Ca^{2+} (left, bottom) and with 0.5 μM intracellular Ca^{2+} (right, bottom), show that 16B-shRNA #2 and #5 reduced CaCC in hippocampal neurons by ~80% at positive voltages. *$p < 0.01$. (G) TMEM16B mRNA expression in mouse dentate granule cells, hilar interneurons, CA1 pyramidal neurons (top) and CA3 pyramidal neurons (bottom) as revealed by *in situ* hybridization. (H) TMEM16B protein is detected in cultured hippocampal neurons at 13, 15, and 17 DIV by western blotting. * indicates a non-specific band. Bottom panel is the neuron-specific β-tubulin as a loading control. See Supplemental Figure 3B for antibody specificity controls.

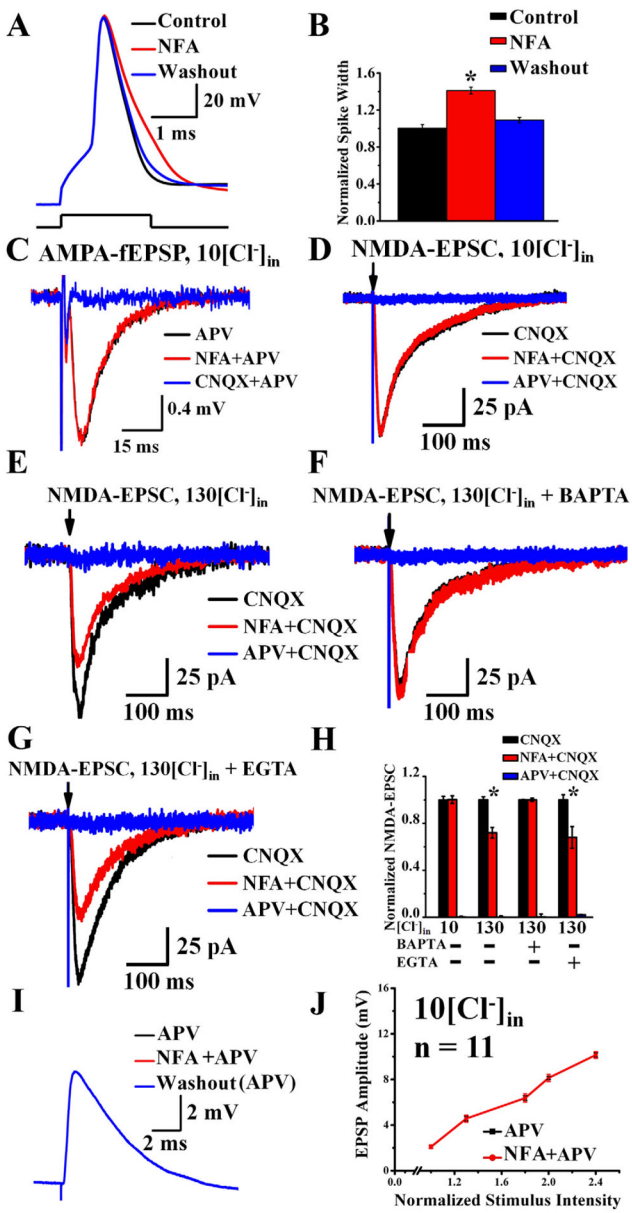

Figure 5.

CaCC shortens the duration of action potentials recorded in CA3 pyramidal neurons, but does not affect transmitter release from their axon terminals upon stimulation of Schaffer collaterals (acute slices, 35°C). (A–B)Reducing CaCC in CA3 neurons in acute hippocampal slices with 100 μM NFA (red) slows the action potential repolarization compared to action potentials before applying NFA (control, black) and after washout of NFA (blue) (A). (B) NFA increases CA3 spike duration. Control, black, 0.99 ± 0.04 ms; NFA, red, 1.41 ± 0.036 ms; n = 10, * $p < 0.01$. See Supplemental Figure 1H for time course plot and experimental details, Supplemental Figure 2 and 4 for controls of the NFA effect. (C) In the presence of 100 μM APV, the AMPA-fEPSP (black) induced by 10 nerve stimuli at 10 Hz was not altered by 100 μM NFA (red) (n = 7, $p = 0.8$). Blue, 20 μM CNQX applied at the end of the experiment. The 6th response is shown in each case. See Supplemental Figure 1R for time course plot. (D) At the holding potential of −65 mV (E_{Cl} = −64.4 mV with 10 mM $[Cl^{-}]_{in}$), the NMDA-EPSC (black) was not altered by 100 μM NFA (red) (n = 5, $p = 0.2$). Blue, 100

μM APV applied at the end of the experiment (recorded in the presence of CNQX). See Supplemental Figure 1S for time course plot. (E–H) When CaCC contribution is maximized by increasing the driving force for Cl^-(E_{Cl} ~ 0 mV with 130 mM $[Cl^-]_{in}$, holding potential at −65 mV) and removing Mg^{2+} block of NMDA-Rs by using a zero-Mg^{2+}/4 mM Ca^{2+} external solution, 100 μM NFA (red) reduces NMDA-EPSC (black) by 28 ± 4.3% (n = 10, p < 0.05) (E). Blue, 100 μM APV applied at the end of the experiment. See Supplemental Figure 1T for time course plot. (F) Chelating internal Ca^{2+} by including 10 mM BAPTA in a 130 mM $[Cl^-]_{in}$ pipette solution eliminates the effect of 100 μM NFA on NMDA-EPSC (black, 20 μM CNQX; red, 100 μM NFA + 20 μM CNQX; blue, 100 μM APV + 20 μM CNQX; n = 10, p = 0.13). See Supplemental Figure 1U for time course plot. (G) With 10 mM EGTA in a 130 mM $[Cl^-]_{in}$ pipette solution, 100 μM NFA (red) reduces NMDA-EPSC (black) by 32 ± 9% (n = 5, p < 0.01). Blue, 100 μM APV applied at the end of the experiment. See Supplemental Figure 1V for time course plot. (H) CaCC contributes to NMDA-EPSC when there is maximal driving force for Cl^- (Figure 5E, n = 10, p < 0.05) and when there is Ca^{2+} influx through NMDA-Rs (Figure 5G, n = 5, p < 0.01). Unlike BAPTA that quickly chelates Ca^{2+} (Figure 5F, n = 10), the slow Ca^{2+} chelator EGTA cannot eliminate CaCC modulation of NMDA-EPSC (Figure 5G, n = 5). (I) AMPA-EPSPs recorded from CA1 neurons (black) by stimulating axons of CA3 neurons are not affected by the NFA block of CaCCs (red). These traces are superimposed with the AMPA-EPSP recorded after washout of NFA (blue). See Supplemental Figure 1W for time course plot. (J) Blocking CaCC with NFA had no effect on pharmacologically isolated AMPA-EPSPs regardless of stimulation intensities or AMPA-EPSP amplitudes (n = 11, p > 0.05). See Supplemental Figure 5 for NFA effect on pharmacologically isolated NMDA-fEPSP.

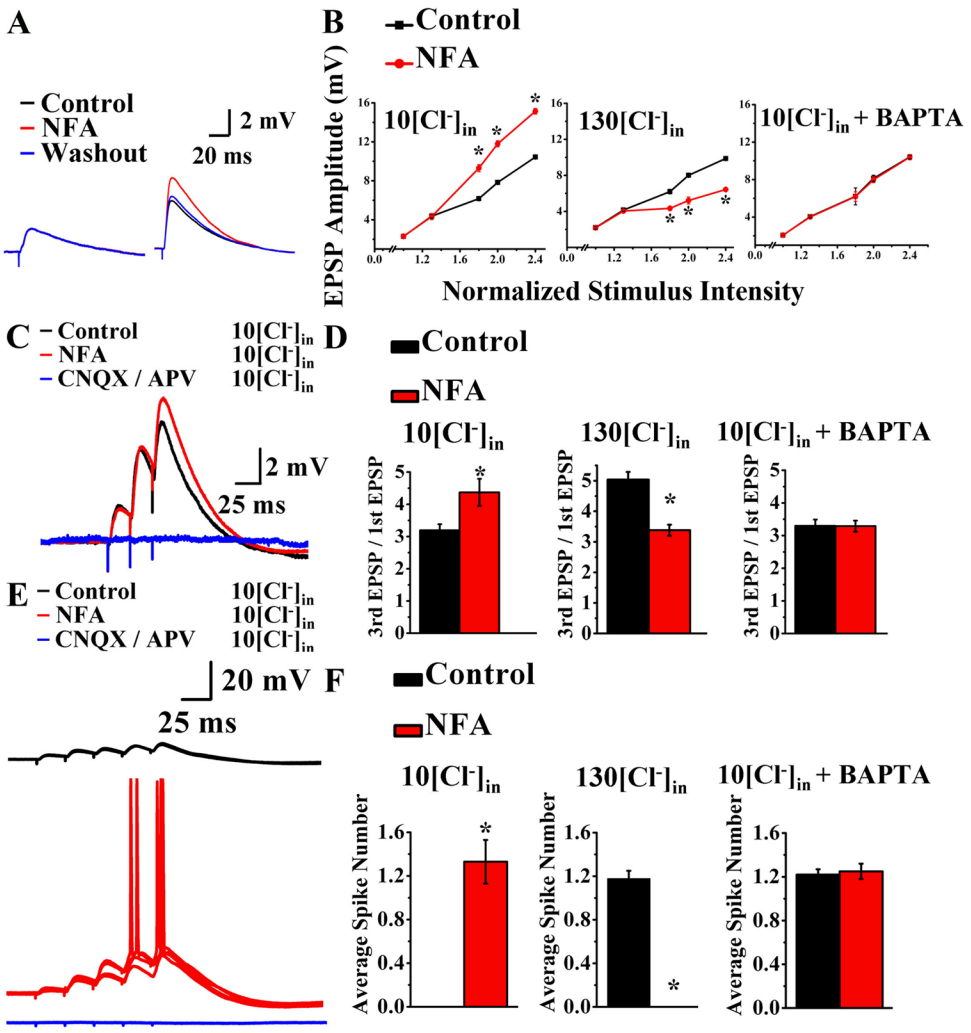

Figure 6.

CaCC activation by Ca^{2+} influx through NMDA-R provides a brake to excitatory synaptic responses, temporal summation, and EPSP-spike coupling (acute slices, 35°C). (A) 100 μM NFA (red) increases the amplitude of large (6 mV) EPSP (right) to 147 ± 2.9% of control, n = 10, $p < 0.05$) (Supplemental 1X) without affecting small (left, n = 10, $p > 0.05$) excitatory synaptic potentials. (B) Reducing CaCC with 100 μM NFA amplifies the larger EPSPs under physiological conditions (left, n = 10, $p < 0.05$), but dampens the larger EPSPs in the presence of 130 mM $[Cl^-]_{in}$ (middle, n = 9, $p < 0.05$). 100 μM NFA has no effect on EPSP amplitude when BAPTA is included with 10 mM $[Cl^-]_{in}$ to chelate Ca^{2+} (right, n = 16, $p > 0.05$). The input-output relations summarize averages of ten recordings in each condition. * $p < 0.05$. See Supplemental Figure 1X–Z for time course plots, Table 1 and Supplemental Information for experimental details. (C) A burst of three nerve stimuli at 40 Hz results in EPSPs that summate and grow progressively. Reducing CaCC with 100 μM NFA (red) enhances the summation efficacy (the ratio of third EPSP over first EPSP) while leaving the first EPSP (EPSPs ≤ 2 mV) unchanged (black, control prior to NFA application). Blue, 20 μM CNQX and 100 μM APV application at the end of the experiment. (D) Reducing CaCC with 100 μM NFA enhances summation and increases the $3^{rd}/1^{st}$ EPSP ratio under physiological conditions (left, n =8, $p < 0.01$), but has the opposite effect in 130 mM $[Cl^-]_{in}$ (middle, n =9, $p < 0.01$). 100 μM NFA has no effect on EPSP summation when BAPTA is

included with 10 mM $[Cl^-]_{in}$ to chelate Ca^{2+} (right, n =5 $p > 0.05$). See Supplemental Figure 1A′-C′ for time course plots, Table 1 and Supplemental Information for experimental details. (E) A burst of five nerve stimuli at 40 Hz generates EPSPs that summate to reach the threshold after (red) but not before (black) application of 100 μM NFA. Blue, 20 μM CNQX and 100 μM APV application at the end of the experiment. Five superimposed recordings are shown. (F) Reducing CaCC with 100 μM NFA enhances EPSP-spike coupling under physiological conditions (left, n = 7, $p < 0.01$), but dampens EPSP-spike coupling in 130 mM $[Cl^-]_{in}$ (middle, n = 8, $p < 0.01$). 100 μM NFA has no effect on EPSP-spike coupling when BAPTA is included with 10 mM $[Cl^-]_{in}$ to chelate Ca^{2+} (right, n = 5, $p > 0.05$). See Supplemental Figure 1D′–F′ for time course plots and Supplemental Figure 6 for NFA effect on pharmacologically isolated NMDA-EPSP spike coupling.

Table 1

CaCC modulates action potential duration, EPSP amplitude and temporal summation, and EPSP-spike coupling

All experiments included in this table were done in acute slices at 35°C. For physiological Cl^- conditions: 10 mM $[Cl^-]_{in}$ and 129 mM $[Cl^-]_{out}$ for E_{Cl}= −64.4 mV. To prevent internal calcium rise, 10 mM BAPTA was added to the pipette solution to chelate internal Ca^{2+}. Controls with inverted Cl^- gradient for experiments involving action potential (generated via 2 ms current injection) had 130 mM $[Cl^-]_{in}$ and 15 mM $[Cl^-]_{out}$ (E_{Cl} = + 54 mV). Controls with inverted Cl^- gradient for experiments involving EPSPs (generated by stimulation of Schaffer collaterals) had 130 mM $[Cl^-]_{in}$ and 130 mM $[Cl^-]_{out}$ (E_{Cl} = 0 mV). Measurements showing statistically significant effects of NFA are in bold. See Supplemental Figure 2 for raised internal chloride concentration and BAPTA controls.

	Low $[Cl^-]_{in}$		**High $[Cl^-]_{in}$**		**Low $[Cl^-]_{in}$ + BAPTA**	
100 μM NFA	**–**	+	**–**	+	**–**	+
Spike duration (ms)	**0.97 ± 0.09**	**1.32 ± 0.10**	**1.83 ± 0.04**	**1.43 ± 0.03**	2.08 ± 0.05	2.03 ± 0.03
	(n = 6, p < 0.001)		**(n = 6, p < 0.001)**		(n = 5, p = 0.39)	
EPSP amplitude (mV)	**6.17 ± 0.21**	**9.30 ± 0.36**	**6.20 ± 0.25**	**4.34 ± 0.24**	6.21 ± 0.90	6.18 ±0.51
	(n = 10, p < 0.05)		**(n = 9, p < 0.05)**		(n = 6, p = 0.42)	
3rd EPSP/1st EPSP (temporal summation)	**3.19 ± 0.19**	**4.27 ± 0.42**	**5.04 ± 0.25**	**3.38 ± 0.18**	3.30 ± 0.19	3.29 ± 0.17
	(n = 8, p < 0.01)		**(n = 9, p < 0.01)**		(n = 5, p = 0.95)	
Voltage Threshold						
2 ms current to induce spike (mV)	−37.42 ± 1.79	−36.66 ± 1.32	−54.65 ± 1.27	−53.91 ± 1.59	−36.21 ± 1.67	−35.16 ± 1.73
	(n = 9, p = 0.3)		(n = 12, p = 0.22)		(n = 8, p = 0.4)	
Single EPSP to spike (mV)	**−42.45 ± 0.71**	**−45.11 ± 0.62**	**−53.71 ± 1.1**	**−50.29 ± 1.12**	−43.37 ± 0.54	−43.11 ± 0.55
	(n = 19, p < 0.01)		**(n = 12, p < 0.01)**		(n = 6, p = 0.4)	
Burst of EPSPs to spike (mV)	**−43.75 ± 0.66**	**−46.56 ± 0.51**	**−55.95 ± 0.54**	**−53.01 ± 0.82**	−46.65 ± 0.25	−46.18 ± 0.32
	(n = 9, p < 0.01)		**(n = 8, p < 0.05)**		(n = 5, p = 0.3)	